International Journal of GEOMATE, March, 2026 Vol.30, Issue 139, pp.77-85
ISSN: 2186-2982 (P), 2186-2990 (O), Japan, DOI: https://doi.org/10.21660/2026.139.5364
Geotechnique, Construction Materials and Environment

NUMERICAL ANALYSIS OF SMALL-SCALE EARTH RETAINING STRUCTURES DURING LIQUEFACTION

* Kakuta Fujiwara [1]

[1]Graduate School of Engineering, Tokai University, Japan

*Corresponding Author, Received: 28 Nov. 2025, Revised: 26 Dec. 2025, Accepted: 27 Dec. 2025

ABSTRACT: In repair works for underground pipelines, lightweight sheet piles are frequently used for excavations with depths of approximately 1–2 m. Because these structures are temporary and small in scale, the embedment length is generally short to facilitate rapid and easy construction. This study performs numerical analyses of small-scale earth-retaining structures under seismic conditions. The target ground is assumed to be sandy and saturated soil in a coastal area, and soil liquefaction is considered in the analysis. The target structure is assumed to have an excavation depth of 2.0 m and an embedment depth of 0.5 m. Based on this reference model, additional simulations were conducted to investigate the effects of four factors: (1) the presence or absence of liquefaction, (2) variations in strut spacing, (3) the application of surcharge loads, and (4) differences in input seismic motions. The results indicate that liquefaction causes uplift of the entire structure and increases the stresses acting on structural components such as struts and walers. The stresses induced in the structural members increase with both increasing strut spacing and higher peak accelerations of the input seismic motion. Furthermore, when a surcharge load is applied only to one side of the ground surface, asymmetric ground deformation occurs, resulting in deformation of the excavation space. Doubling the strut spacing, applying a surcharge load on the ground surface, and the occurrence of an L2-class earthquake all resulted in axial forces in the strut exceeding the allowable values.

Keywords: Small-scale excavation, Retaining wall, Numerical analysis, Earthquake, Liquefaction

1. INTRODUCTION

Ground deformation has been reported even in small-scale and shallow excavations, such as utility trench works with excavation depths of 1–2 m. Field measurements and experimental studies have shown that ground settlement and lateral deformation can occur around shallow excavations, potentially affecting adjacent ground and buried structures [1]. These findings indicate that deformation control is an important issue not only for deep excavations but also for small-scale construction projects.

In coastal construction areas, sandy ground conditions are common, and the soil generally exhibits low or negligible cohesion. Furthermore, when the sand is saturated, the risk of liquefaction during earthquakes becomes a critical concern, even for shallow excavations.

For excavation construction safety, lightweight sheet-pile with strut and waler, have been commonly used. This system provides improved stiffness and resistance against deformation compared with single retaining walls. Fig. 1 shows a photograph provided to explain the names of each structural member. In this photograph, the excavation depth is 1.3 m and the excavation width is 0.7 m. Both sides of the excavation are retained by aluminum sheet piles. Hooks are attached to the aluminum sheet piles, and walers are placed on these hooks. Struts, which function as compression members, are installed between the walers to prevent the sheet piles from inclining toward the excavation side. In the present study, a sand ground is considered, and therefore the ground conditions differ from those shown in the photograph.

Considerable research for this type of structure has been conducted under static conditions through numerous theoretical and physical models [2-5]. Since this type of structure is mainly used as a temporary construction facility, the probability of encountering a strong earthquake during its service period has been considered to be low, and therefore its dynamic behavior has not been extensively investigated. However, given the very large number of such construction projects, it is inevitable that some of these structures will experience seismic events. Consequently, studies focusing on their behavior under earthquake loading have gradually been conducted [6-7].

Konai et al. conducted systematic investigations on this type of structure through 1-g small-scale model tests and corresponding numerical simulations, covering both static and dynamic behavior. The study showed that in a post-seismic condition, when other factors were constant, lateral displacement, bending moment, strut forces and maximum ground surface displacement increased with excavation depth and the amplitude of base acceleration [8].

Konai et al. also conducted model tests and corresponding numerical simulations considering liquefaction. The pore water pressures developed in the soil are found to influence the behavior of the braced wall structures during a dynamic event. It is

found that the excess pore water pressure development in the soil below the excavation is higher compared to the soil beside the walls. Thus, the soil below the excavation level is more susceptible to the liquefaction compared to the soil beside the walls [9].

However, in this study [9], the representative prototype excavation depth and embedment length were both approximately 5 m. On the other hand, shallow excavations with depths of about 1–2 m was not examined. In such shallow excavations, construction simplicity is often prioritized in practice, which tends to result in shorter embedment lengths (0.2–1m). Due to the relatively small embedment length compared with the excavation depth, it can be regarded as a potentially unsafe structure due to the relatively short embedment length.

Therefore, this study performs numerical analyses of earth-retaining works for shallow excavation under seismic conditions. The target site is assumed to be a sandy, saturated ground near the coast, and the numerical analysis incorporates the effects of liquefaction. Additional simulations were also conducted to compare four scenarios: without considering liquefaction, with varying spacing of struts, with the application of surcharge loads and varying input motions.

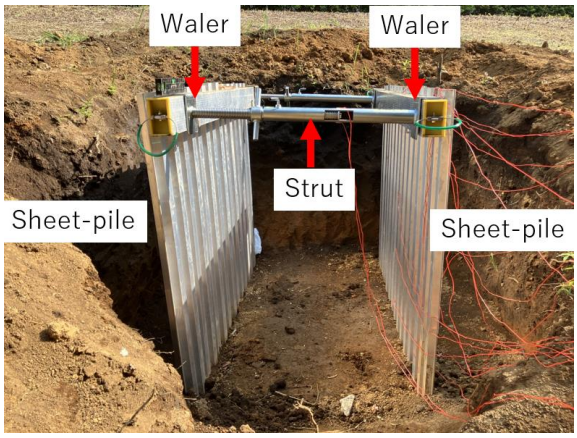

Fig. 1 Small-scale excavation with retaining wall

2. RESEARCH SIGNIFICANCE

This study provides a novel numerical evaluation of small-scale earth-retaining structures with shallow excavation depths and short embedment lengths under liquefaction-induced seismic conditions. Unlike previous studies focusing on large or permanent structures, this research clarifies the deformation mechanisms, uplift behavior, and stress concentration in temporary retaining systems commonly used in practice. The findings offer original insights into the safety limits of such structures during strong earthquakes.

3. NUMERICAL CONDITION

The numerical analyses were conducted using LIQCA3D20. The target embankment was constructed on two layers of sandy ground shown as Fig. 2. Aluminum sheet piles were installed facing each other to construct an earth-retaining system, followed by excavation to form a space measuring 2 m in depth and 2 m in width. The embedment of the sheet-pile is 0.5m. The ground was discretized into 5400 cuboid elements. To perform numerical analysis, parameters such as dimensions, soil parameters, and countermeasures needed to be specified. The following sub-sections describe the ground condition, these parameters and their corresponding values.

3.1 Soil

The ground condition was a representative loose sandy soil with a relative density (Dr) of 40 %. The soil parameters used in the numerical model were shown in Table 1. Sand above the groundwater was modeled as dry, while that below was modeled as saturated. The soil parameter values were inferred and determined from the academic paper by Fujiwara et al [10]. The sand layers were modeled as elasto-plastic models created [11, 12], which is often used to model a loose sand layer. This model represents sand behavior resulting from an increase in excess pore water pressure which causes motion, making the sand soft, and finally causing liquefaction.

3.2 Structural Component

The sheet piles are installed facing each other and are supported near their top ends by struts. The sheet piles are also connected in the longitudinal direction by walers. Table 2 shows the actual cross-sectional properties, and the corresponding values adopted in the numerical model for the sheet piles, struts and walers. The sheet piles were 2.5 m long, with an embedment depth of 0.5 m. The sheet-piles were modeled by cuboid meshes with linear elastic material having no yield. The mesh thickness was set to 20 mm, and the Young's modulus was set to 1.52 x 10^8 kN/m^2 so that the flexural rigidity would be equivalent to that of the sheet pile. The density was set to 0.75 g/cm^3 to match the mass of the sheet pile, thereby ensuring that the inertial force during seismic loading would also be equivalent.

The strut and waler were modeled using beam elements. The strut was connected at both ends to the sheet piles at positions 0.5 m below their tops (x = 0 m). The walers were connected to the sheet piles in the longitudinal direction at positions 0.5 m below their tops. The strut and the waler were HKS140-210C and HAH1207-1.8, respectively, both manufactured by Hoshin Co., Ltd. The allowable axial force and the allowable bending moment specified in the product specifications were 39.2 kN and 9.9 kNm, respectively. However, in the present

analysis, the strut and the waler were modeled as elastic materials, and the product strength limits were not taken into account.

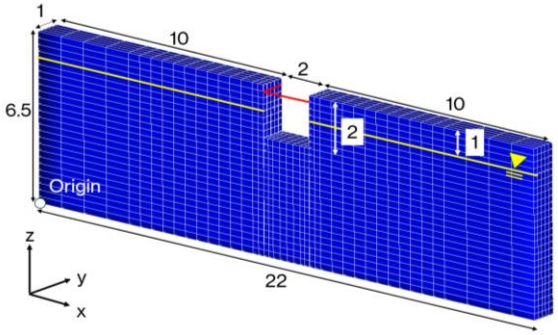

(a) Schematic view (without sheet-pile)

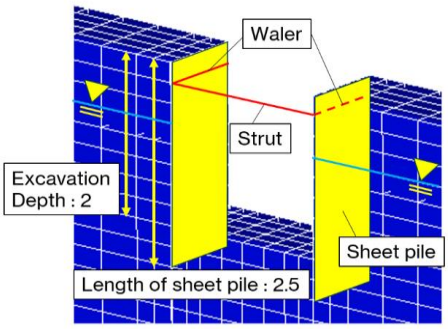

(b) Enlarged view

Fig. 2 The numerical model for Case 1 (Unit: m)

Table 1 Soil parameter

Initial stress analysis		Unit	Value
Density	ρ	t/m^3	1.8
Young's moduls	E_0	kN/m^2	5508
Poisson's ratio	ν		0.33
Cohesion	C	kN/m^2	0
Friction angle	ϕ	degree	32
Dynamic analysis			
Coefficient of permeability	k	m/s	2.0×10^{-4}
Initial void ratio	e_0		0.821
Compression index	λ		0.015
Swelling index	κ		0.002
	OCR*		1
Initial elastic shear modulus rat	G_0/σ'_m		1000
Stress ratio at critical state	M^*_m		0.909
Stress ratio at failure	M^*_f		1.122
	B^*_0		7000
Hardening parameter	B^*_1		50
	C_f		2000
Dilentancy parameter	D_0		3
	n		3
Reference strain parameter	γ^{P*}		0.01
	γ^{E*}		0.02

Table 2 Parameters for structural component

Sheet-pile		Unit	Value
Density	ρ	t/m^3	0.75
Young's moduls	E_0	kN/m^2	1.52×10^{8}
Poisson's ratio	ν		0.33

Strut		Unit	Value
Density	ρ	t/m^3	7.8
Young's moduls	E_0	kN/m^2	2.0×10^{8}
Poisson's ratio	ν		0.33
Area	A	m^2	4.56×10^{-4}
Second moment of area	I	m^4	1.18×10^{-7}

Waler		Unit	Value
Density	ρ	t/m^3	2.7
Young's moduls	E_0	kN/m^2	6.86×10^{7}
Poisson's ratio	ν		0.33
Area	A	m^2	2.32×10^{-3}
Second moment of area	I	m^4	2.17×10^{-6}

Table 3 Numerical case

Case	Liquefaction	Spacing between struts	Vertical load	Input motion
1	✓	2 m	No	L1
2	No	2 m	No	L1
3-1	✓	1 m	No	L1
3-2	✓	4 m	No	L1
4-1	✓	2 m	Both sides	L1
4-2	✓	2 m	One side	L1
5-1	✓	2 m	No	Kumamoto
5-2	✓	2 m	No	Ishikawa

3.3 Boundary Condition

The coordinate system was set up with the y-axis extending along construction longitudinal direction, the x-axis perpendicular to the y-axis in the horizontal plane, and the z-axis pointing vertically upward. The z-x dimensions of the model were as follows: 22 m in the x-direction and 6.5 m in the z-direction.

Taking symmetry considerations into account, fixed boundary conditions were assigned at the locations of the side nodes in the x-direction, at x = 0 m and x = 22 m. In the y-direction, fixed boundary conditions were assigned at the locations of the side nodes at y = 0 m and 1 m. In the z-direction, the bottom nodes were fixed at z = 0 m in all cases.

3.4 Numerical Case

Numerical cases are listed in Table 3. For Case 1, the groundwater table is at a depth of 1 m, and the spacing of the struts is 2 m; this is taken as the basic structure. For Case 2, there is no groundwater, and the entire ground is assumed to be dry sand. Liquefaction is not considered. For Cases 3-1 and 3-2, the spacing of the struts is 1 and 4 m, respectively. For Case 4-1, a vertical load is applied to both sides of the ground surface. For Case 4-2, the vertical load is applied to

the right side of the ground surface. The vertical load is set to 10 kN/m^2, which is the design load specified in [13], taking into account the weight of construction equipment and materials. For Cases 5-1 and 5-2, different input motions, as explained in the following section, were applied to the Case 1 structure to clarify the differences in structural behavior.

3.5 Input Motion

The dynamic analyses were conducted based on the results of the initial analyses, using three input motions: a Level 1 earthquake motion at Kisarazu port, the 2016 Kumamoto earthquake, and the 2024 Ishikawa earthquake.

The Level 1 earthquake motion, publicly released for coastal areas, was employed, as shown in Fig. 3(a). The data were provided by the National Institute for Land and Infrastructure Management (NILIM) [14].

The Kumamoto earthquake motion was observed in Uki City in the NS direction, and the Ishikawa earthquake motion was observed in the Noto Peninsula in the EW direction, as shown in Fig. 3(b) and Fig. 3(c), respectively. These records were provided by the Japan Meteorological Agency (JMA) [15]. The maximum accelerations of the Level 1, Kumamoto, and Ishikawa earthquake motions were 1.49 m/s², 4.90 m/s², and 5.61 m/s², respectively. The dominant frequencies of all three earthquake motions were approximately 1.13 Hz, 0.66 Hz, 0.46 Hz. The Kumamoto and Ishikawa earthquake records can be regarded as strong ground motions comparable to Level 2 earthquake motions.

The Newmark method was used to solve the responses of the soil and the structure. An incremental time interval of 0.005 s was used, while a value of 0.3025 was used for the coefficient β in the Newmark method and the value of γ was set at 0.6. We used a stiffness-proportional coefficient of 0.003 for Rayleigh damping.

4. NUMERICAL RESULT

In this chapter, the results of the numerical analysis are explained with a focus on the presence or absence of liquefaction (Case 2), the spacing of struts (Cases 3-1 and 3-2), the presence or absence of surcharge loading (Cases 4-1 and 4-2), and the difference of input motions (Cases 5-1 and 5-2), compared to the basic structure (Case 1).

4.1 The Presence and Absence of Liquefaction

For Cases 1 and 2, the deformations with excess pore water pressure ratio, corresponding to the end of shaking (t = 163 s), are represented by the heat maps shown in Fig. 4. The excess pore water pressure ratio is obtained by dividing the excess pore water pressure by the initial effective stress. In Case 1, the entire ground underwent significant deformation due to liquefaction. In contrast, in Case 2, no liquefaction was observed, and large deformation occurred only in the vicinity of the sheet pile. In both cases, due to the restraint provided by the struts near the top, the sheet pile exhibited bulging deformation around their mid-height. Regarding the behavior in the vertical direction, in Case 1, the liquefied ground flowed beneath the sheet pile, resulting in an upward thrust that lifted the entire sheet pile; however, such behavior was not observed in Case 2. Although the embedment length was relatively short in both Cases 1 and 2, structural stability was maintained.

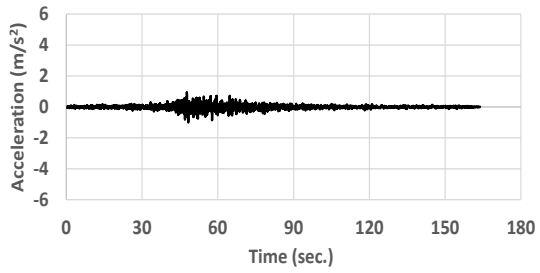

(a) L1 earthquake

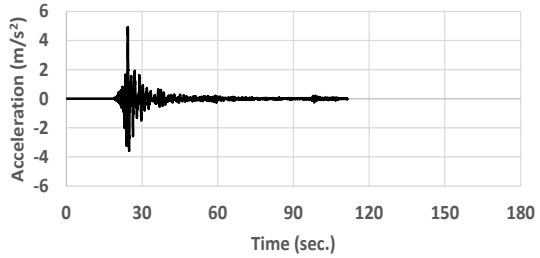

(b) Kumamoto earthquake

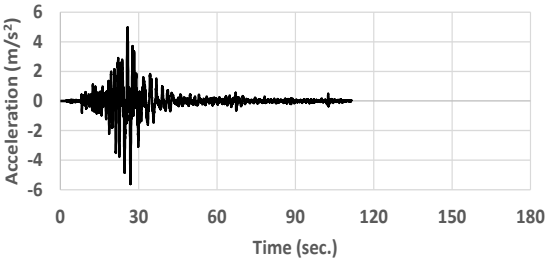

(c) Ishikawa earthquake

Fig. 3 Input motion

The time histories of the axial force in the strut and the maximum bending moment in the waler are presented in Fig. 5, respectively. Compressive axial force was generated in the strut to resist the deformation of the sheet piles. The waler exhibited bending deformation as a beam supported at two points, with the supports located at the intersections with the strut. The maximum bending moment developed at the midpoint between the supports (y = 1 m). In Case 1, the strut experienced a maximum axial compression force of 36 kN and a maximum bending moment of 2.4 kNm, both of which occurred

around 50 seconds, coinciding with the peak of the input acceleration. In Case 2 as well, the axial force and bending moment in the strut reached their maximum value around 50 seconds; however, these were significantly smaller than those in Case 1, at 16 kN and 1.3 kNm, respectively. Notably, little significant vibrational components were observed. In addition, in both Cases 1 and 2, the axial force in the strut and the bending moment in the waler remained below the allowable values specified in the product specifications.

Fig. 6 shows the depth-wise distribution of horizontal and vertical displacements of both sheet pile walls at y =1 m. The horizontal displacement was generally similar between Case 1 and Case 2. However, in Case 1, an upward vertical displacement (uplift) was observed, whereas no such uplift was seen in Case 2.

4.2 The Spacing of Struts

For Cases 3-1 and 3-2, the deformations with excess pore water pressure ratio (t = 163 s) are represented in Fig. 7. In comparison with Case 1, little difference was observed in the occurrence of liquefaction and the deformation of the ground.

The time histories of the axial force in the strut and the maximum bending moment in the waler are presented in Fig. 8. In Cases 3-1 and 3-2, the strut experienced a maximum axial force of 20 kN and 62 kN, and a maximum bending moment of 0.7 kNm and 6.4 kNm, respectively. The axial force generated in the strut was approximately proportional to the spacing between them. The bending moment in the waler increased more than proportionally with the spacing between the struts, that is, the distance between the supports of the waler, this trend can be attributed to the fact that the bending moment acting on the waler is governed by the square of the strut spacing. In Case 3-2, the axial force in the strut exceeded the allowable value specified in the product specifications, indicating that caution is required when increasing the spacing between struts.

Fig. 9 shows the depth-wise distribution of horizontal and vertical displacements of both sheet pile walls at the plane in the middle of the waler. In Case 3-2, where the spacing between struts is large, slightly larger horizontal displacements were observed at the top of the sheet pile. No significant differences were observed in other displacements.

4.3 The Surcharge Loading

For Cases 4-1 and 4-2, the deformations with excess pore water pressure ratio (t = 163 s) are represented in Fig. 10. Due to the application of a surface surcharge, the ground deformation in these cases was larger than that in Case 1. In particular, in Case 4-2, the eccentric load caused the ground to deform predominantly in the leftward direction.

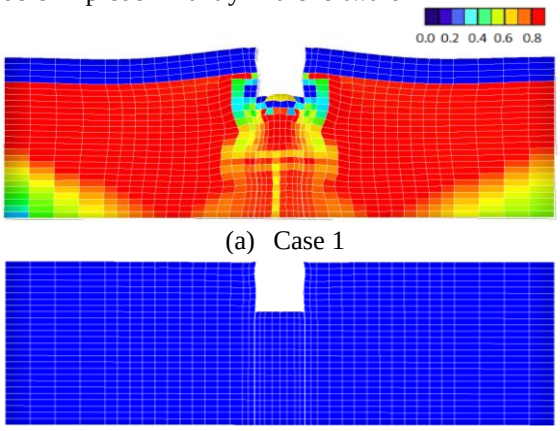

(a) Case 1

(b) Case 2

Fig. 4 The deformation with the excess pore water pressure ratio after shaking (Cases 1 and 2)

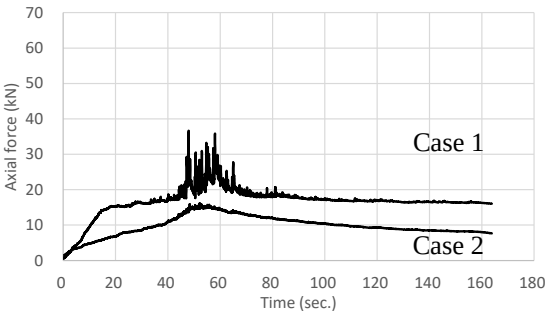

(a) Axial force in the strut

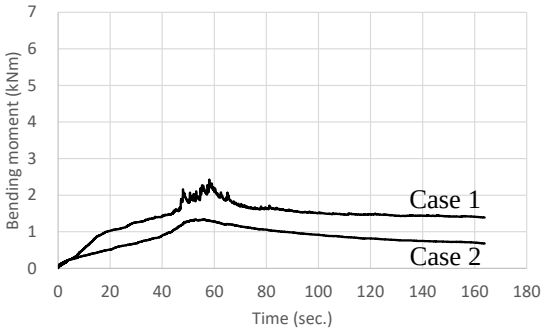

(b) Maximum bending moment in the welder

Fig. 5 The time histories of the internal forces in structural components (Cases 1 and 2)

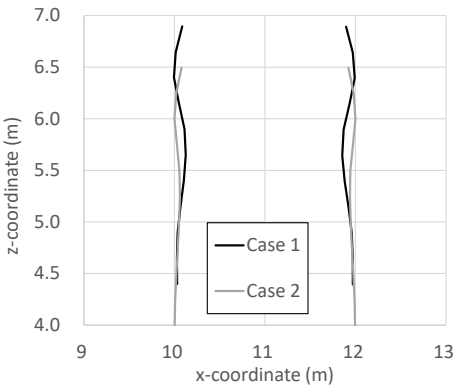

Fig. 6 Horizontal and vertical displacement in both sheet piles (Cases 1 and 2)

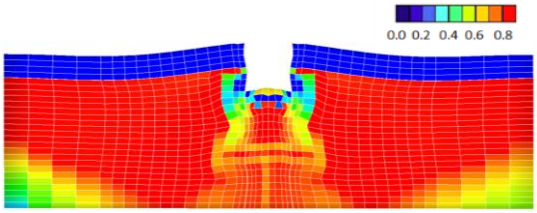

(a) Case 3-1

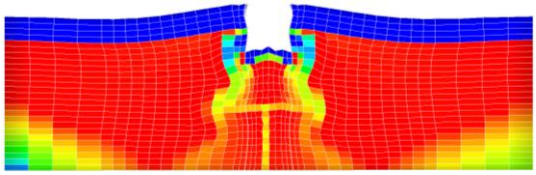

(b) Case 3-2

Fig. 7 The deformation with the excess pore water pressure ratio after shaking (Cases 3-1 and 3-2)

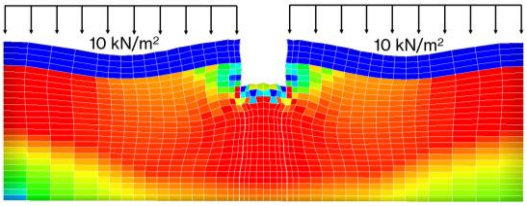

(a) Case 4-1

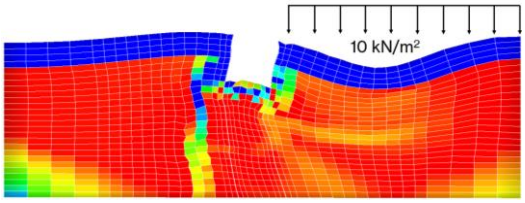

(b) Case 4-2

Fig. 10 The deformation with the excess pore water pressure ratio after shaking (Cases 4-1 and 4-2)

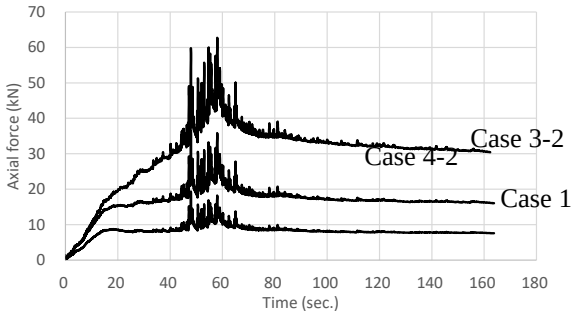

(a) Axial force in the strut

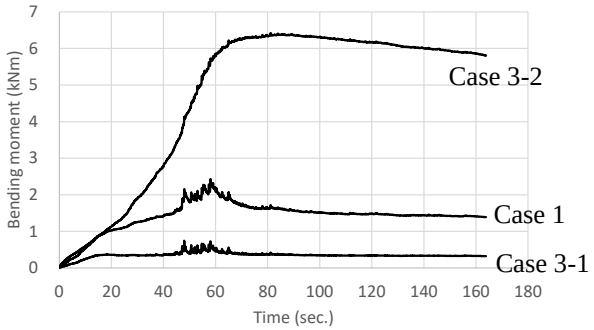

(b) Maximum bending moment in the welder

Fig. 8 The time histories of internal forces in structural components (Cases 1, 3-1 and 3-2)

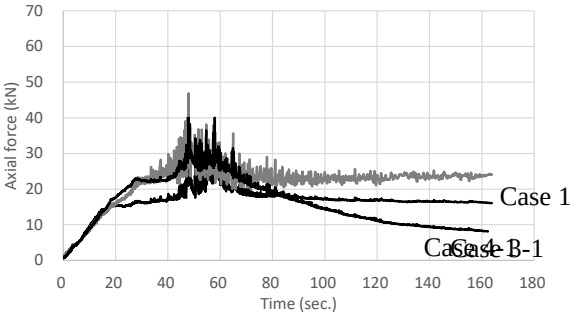

(a) Axial force in the strut

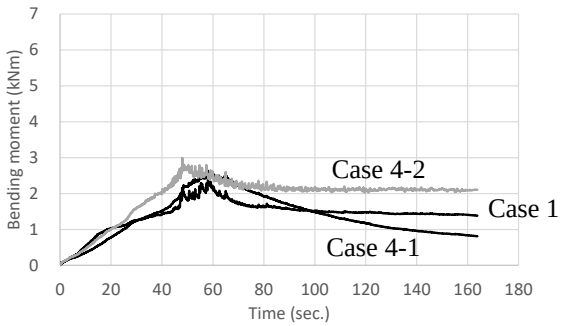

(b) Maximum bending moment in the welder

Fig. 11 The time histories of internal forces in structural components (Cases 1, 4-1 and 4-2)

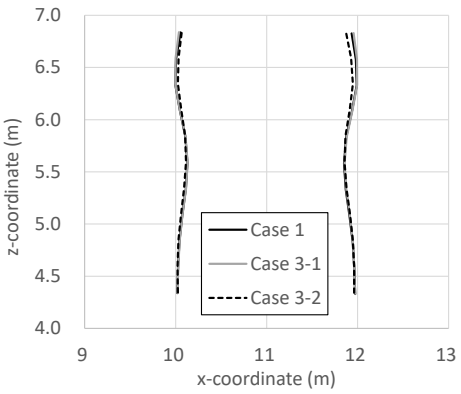

Fig. 9 Horizontal and vertical displacement in both sheet piles (Cases 1, 3-1 and 3-2)

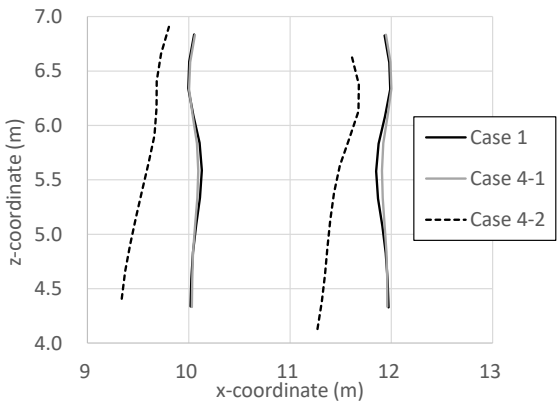

Fig. 12 Horizontal and vertical displacement in both sheet piles (Cases 1, 4-1 and 4-2)

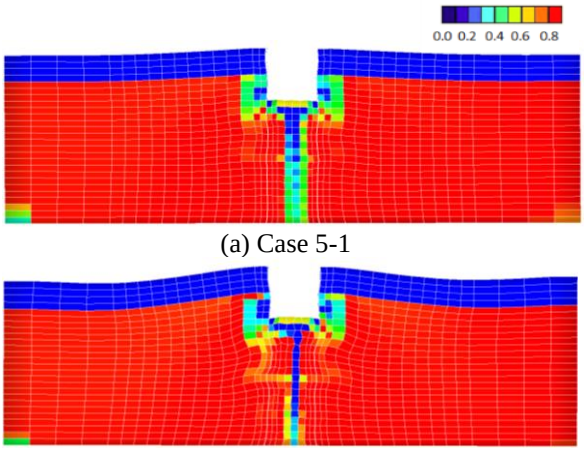

(a) Case 5-1

(b) Case 5-2

Fig. 13 The deformation with the excess pore water pressure ratio after shaking (Cases 5-1 and 5-2)

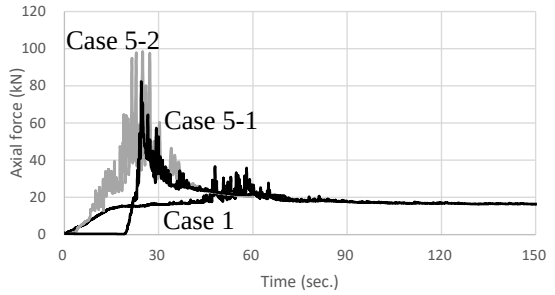

(a) Axial force in the strut

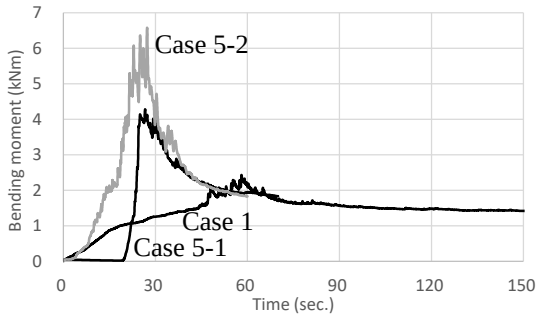

(b) Maximum bending moment in the welder

Fig. 14 The time histories of internal forces in structural components (Cases 1, 5-1 and 5-2)

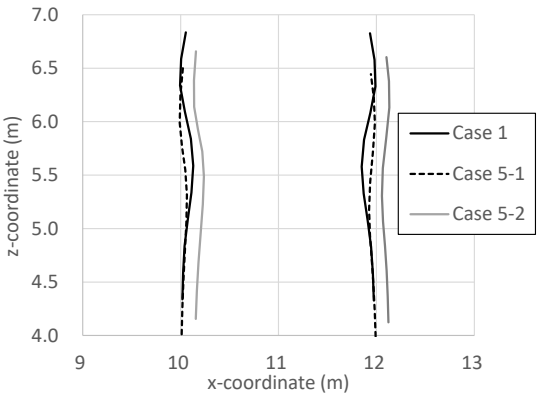

Fig. 15 Horizontal and vertical displacement in both sheet piles (Cases 1, 5-1 and 5-2)

The time histories of the axial force in the strut and the bending moment in the waler at y=1 m are presented in Fig. 11. The strut experienced a maximum axial force of 41 kN and 47 kN and a maximum bending moment of 2.6 kNm and 3.0 kNm. Compared to Case 1 without loading, the axial forces in the struts and the bending moments in the waler increased in Cases 4-1 and 4-2, where loading was applied. The axial forces in the strut exceeded the allowable value specified in the product specifications.

Fig. 12 shows the depth-wise distribution of horizontal and vertical displacements of both sheet pile walls at y =1 m. Little significant differences were observed between Cases 1 and 4-1. In Case 4-2, the two sheet piles moved while undergoing rotation. The soil on the loading side pushed against the sheet piles, causing both rows of sheet piles to shift toward the non-loading side. As a result, the working space required for pipe installation and other construction activities was reduced, indicating a potentially hazardous situation.

4.4 Differences Due to Earthquake Motion

For Cases 5-1 and 5-2, the deformations and the excess pore water pressure ratio at the end of the earthquake are shown in Fig. 13.

In Case 1, liquefaction did not occur in the lower left and lower right parts of the saturated sand layer. In contrast, in Cases 5-1 and 5-2, the input earthquake motions were larger, and liquefaction occurred over almost the entire saturated sand layer. In Case 5-2, which had the largest maximum acceleration, greater deformation of the ground surface was also observed.

The time histories of the axial force in the strut and the bending moment in the waler at y = 1 m are presented in Fig. 14. The strut experienced maximum axial forces of 36 kN, 82 kN, and 98 kN for Cases 1, 5-1, and 5-2, respectively, while the maximum bending moments in the waler were 2.4 kNm, 4.3 kNm, and 6.6 kNm for the same cases. Although the axial forces in the strut and the bending moments in the waler in Cases 5-1 and 5-2 were larger than those in Case 1, the differences were not proportional to the ratios of the maximum accelerations (Cases 1, 5-1, and 5-2 = 1.5 : 4.9 : 5.6). The axial force in the strut and the bending moment in the waler are induced by inertial forces during the earthquake and by increased earth pressure associated with liquefaction. However, since the ground in Case 1 was also sufficiently liquefied, the contribution of the latter was similar among the cases, resulting in relatively small differences. The axial forces for Cases 5-1 and 5-2 in the strut exceeded the allowable value specified in the product specifications.

Fig. 15 shows the depth-wise distributions of horizontal and vertical displacements of both sheet

pile walls at y = 1 m. Compared with Case 1, the sheet pile walls in Cases 5-1 and 5-2 exhibited larger horizontal and vertical displacements. Deformation of the excavation space poses a potential hazard to workers, and the numerical analyses indicate that the proposed method cannot ensure safety against L2-class earthquakes.

4.5 Limitation

In the present analysis, the structural members were assumed to behave elastically; however, several cases showed axial forces in the strut exceeding the allowable values specified in the product specifications. As a result, yielding of the strut may occur, and further increases in deformation of the overall structure and the surrounding ground are expected.

5. CONCLUSIONS

This study conducted numerical analysis of small-scale earth retaining works under seismic conditions. The target site is assumed to be sandy and saturated ground, and the numerical analysis takes liquefaction into account. The target structure has a relatively shallow excavation depth, and the embedment length is relatively small compared with the excavation depth. The following results could be gained:

1) In the analysis results for the basic structure, liquefaction of the ground due to the earthquake caused horizontal loads from the soil to act on the two sheet piles and resulted in the compression of the underground space. To resist this, compressive axial force was generated in the strut, and bending moment was induced in the waler.

2) When liquefaction was not considered, the axial force in the struts and the bending moment in the waler were reduced to approximately half. In particular, the dynamic components of these forces were almost eliminated.

3) The axial force generated in the strut was approximately proportional to the spacing between them, while the bending moment in the waler was approximately proportional to the square of the spacing between the struts, that is, the distance between the supports of the waler.

4) Application of the surcharge load to only one side of the ground poses a greater risk of underground space deformation compared to loading on both sides during liquefaction.

5) Doubling the strut spacing, applying a surcharge load on the ground surface, and the occurrence of an L2-class earthquake all resulted in axial forces in the strut exceeding the allowable values. When the excavation “width” is reduced, that is, when the strut length becomes shorter, products with higher allowable axial forces are available. Therefore, if excessive loading on the strut is a concern, revising the excavation width is recommended.

6) For the cases in which the axial force in the strut exceeded the allowable value, yielding of the strut may occur, and further increases in deformation of the overall structure and the surrounding ground are expected.

7) In the future, the validity of the present analytical results will be examined by the authors through model experiments and full-scale construction tests.

6. ACKNOWLEDGMENTS

This study was conducted with a donation from NIPPON STEEL Echo-Tech Corporation, to whom the authors express their sincere gratitude.

7. REFERENCES

1. Franzén, G., Spetz, T. and Sällfors, G., Settlement of sewer pipes in soft clay installed in a trench, in Geotechnical Aspects of Underground Construction in Soft Ground, CRC Press, Rotterdam, 2000, pp. 625–630. https://www.issmge.org/publications/online-library
2. Finno R.J., Harahap I.S. and Sabatini P.J.M., Analysis of Braced Excavations with Coupled Finite Element Formulations, Computers and Geotechnics, Vol. 12, No. 2, 1991, pp. 91–114. http://doi.org/10.1016/0266-352X(91)90001-V
3. Finno R.J. and Harahap I.S., Finite Element Analyses of HDR-4 Excavation, Journal of Geotechnical Engineering, Vol. 117, No. 10, 1991, pp. 1590–1609. http://doi.org/10.1061/(ASCE)0733-9410(1991)117:10(1590)
4. Nakai T., Kawano H., Murata K., Banno M. and Hashimoto T., Model Test and Numerical Simulation of Braced Excavation in Sandy Ground: Influences of Construction History, Wall Friction, Wall Stiffness, Strut Position and Strut Stiffness, Soils and Foundations, Vol. 39, No. 3, 1999, pp. 1–12. http://doi.org/10.3208/sandf.39.3_1
5. Teparaksa J., Soil-retaining structural design and FEM comparison for detected diaphragm wall movement during upward basement construction, International Journal of GEOMATE, Vol. 27, No. 121, 2024, pp. 85-94. https://doi.org/10.21660/2024.121.g12150
6. Chen Y.M., Zhang Z.C. and Liu H.L., Study of the Seismic Performance of Hybrid A-Frame Micropile/MSE (Mechanically Stabilized Earth) Wall, Earthquake Engineering and Engineering Vibration, Vol. 16, No. 2, 2017, pp. 275–295. http://doi.org/10.1007/s11803-017-0382-0
7. Pain A., Choudhury D. and Bhattacharyya S.K., Seismic Passive Earth Resistance Using Modified

Pseudo-Dynamic Method, Earthquake Engineering and Engineering Vibration, Vol. 16, No. 2, 2017, pp. 263–274. http://doi.org/10.1007/s11803-017-0381-1

8. Konai S., Sengupta A. and Deb K., Behavior of braced excavation in sand under a seismic condition: experimental and numerical studies, Earthquake Engineering and Engineering Vibration, Vol. 17, 2018, pp. 311–324. http://doi.org/10.1007/s11803-018-0443-z
9. Konai S., Sengupta A. and Deb K., Behavior of Braced Wall Embedded in Saturated Liquefiable Sand under Seismic Loading, Earthquake Engineering and Engineering Vibration, Vol. 20, No. 2, April 2021, pp. 373–394. http://doi.org/10.1007/s11803-021-2025-8
10. Kakuta Fujiwara, Nanase Ogawa and Kentaro Nakai, 3-D Numerical Analysis of Partial Floating Sheet-pile Method as Countermeasure for Liquefaction, Journal of Japan Society of Civil Engineers, Vol. 9, 2021, pp.138-147. https://www.jstage.jst.go.jp/article/journalofjsce/9/1/9_138/_article
11. Oka F., Yashima A., Shibata T., Kato M., and Uzuoka R., FEM-FDM coupled liquefaction analysis of a porous soil using an elasto-plastic model, Applied Scientific Research, Vol. 52, 1994, pp. 209–245. https://doi.org/10.1007/BF00853951
12. Oka F., Yashima A., Tateishi A., Taguchi Y., and Yamashita A., A cyclic elasto-plastic constitutive model for sand considering a plastic-strain dependence of the shear modulus, Geotechnique, Vol. 49(5), 1999, pp. 661–680. https://doi.org/10.1680/geot.1999.49.5.661
13. Public Interest Incorporated Association –Japan Road Association, Road Earthwork –, Temporary Structure Engineering Guidelines, 1999, pp.156-160.
14. National Institute for Land and Infrastructure Management (NILIM), Technical Information on Coastal Facilities. https://www.ysk.nilim.go.jp/kakubu/kouwan/setu/level1.html
15. Japan Methodological Agency Homepage https://www.data.jma.go.jp/eqev/data/index.html#riyou